

## Topological Degeneracy Induced by Twisting

Han Peng<sup>1,\*</sup>, Qiang Wang<sup>1,\*†</sup>, Meng Xiao<sup>2,3,‡</sup>, Xiayi Wang<sup>1</sup>, Shining Zhu<sup>1</sup>, and Hui Liu<sup>1,§</sup>

<sup>1</sup>National Laboratory of Solid State Microstructures, Jiangsu Physical Science Research Center, School of Physics, Collaborative Innovation Center of Advanced Microstructures, Nanjing University, Nanjing 210093, China

<sup>2</sup>Key Laboratory of Artificial Micro- and Nano-structures of Ministry of Education and School of Physics and Technology, Wuhan University, 430072 Wuhan, China

<sup>3</sup>Wuhan Institute of Quantum Technology, Wuhan 430206, China

 (Received 12 September 2024; revised 19 December 2024; accepted 31 January 2025; published 11 March 2025)

In recent years, twisting has emerged as a new degree of freedom that plays an increasingly important role in Bloch bands of various physical systems. However, there is currently a lack of reports on the nontrivial physics of topological degeneracy in twisted systems. In this Letter, we investigated the intrinsic physical correlation between twisting and topological degeneracy. We found that twisting not only breaks the symmetry of the system but also introduces topological degeneracy that does not exist under the original symmetric system without twisting. Furthermore, the topological degeneracy can be easily tuned through twisting. This new twist-induced topological degeneracy gives rise to a unique polarization-degenerate birefringent medium, wherein the twist angle acts as a novel degree of freedom for dispersion and polarization management of interface states. Exhibiting fascinating properties and experimental feasibilities, our Letter points to new possibilities in the research of various topological physics in twisted photonics.

DOI: [10.1103/PhysRevLett.134.106601](https://doi.org/10.1103/PhysRevLett.134.106601)

*Introduction*—Very recently, the twist angle, as a new degree of freedom, has been widely explored to manipulate quantum materials. The delicate interlayer coupling is controlled by the twist angle, leading to the emergent field of moiré structures [1,2], e.g., the prominent twisted bilayer graphene [3–7]. The moiré physics has also been extended to classical wave systems [8]. In photonics, twist angle can give rise to exotic phenomenon [9–14], including flat band in bilayer photonic crystals [15–19], phase synchronization in nanolasers [20] and many more [21–24]. To date, most of the works on twist photonics have primarily focused on generating flat bands where interlayer couplings intend to introduce gapped phases. However, to the best of our knowledge, there is currently a lack of reports on the nontrivial physics of topological degeneracy in twisted systems.

Topological degeneracies [25–27] (TDs) usually serve as the phase transition points between topological trivial and nontrivial phases, thus play a vital role in identification of various topological phases [28]. Systems exhibiting TDs such as Dirac and Weyl nodes [29,30] are dubbed as topological semimetals. Typical optical systems confined in one direction can also host TDs [31,32], provided that certain symmetries are preserved [33,34]. For example, the Dirac points (DPs) in two-dimensional (2D) photonic

honeycomb lattice are protected by time reversal symmetry and inversion symmetry [35]. Once either symmetry is broken, TDs would be lifted, resulting in gapped phases [36,37]. Therefore, most of the previous works insist on preserving certain symmetries to construct topological degeneracy. There is scarcely any work discussing the opposite physical mechanism about symmetry-breaking induced TDs (in particular, DPs) [38,39], i.e., TDs emerge when certain symmetry is broken.

In this Letter, we investigated the intrinsic physical correlation between twisting and topological degeneracy. Our findings indicate that twisting not only breaks the symmetry of the system but also introduces topological degeneracy that is absent in the original symmetric system without twisting. We present a specifically designed system to demonstrate the twist-induced TDs. The structure consists of two anisotropic metasurfaces separated and sandwiched by photonic crystals (PCs). Two anisotropic interface states (AISs) are supported at the metasurfaces. They coupled to form twisted bilayer AISs (TB AISs) through the PC in between and a band gap opens. By twisting one of the two anisotropic metasurfaces, the up-down mirror symmetry is broken, and intriguingly, two type-II DPs emerge in the momentum space. In other words, mirror symmetry breaking dictates the presence of the DPs. Meanwhile, the position of the DPs can be shifted by tuning the twist angle. Considering the twist angle as an additional dimension besides the 2D momentum space, the Dirac nodes form two nodal lines. These two nodal lines merge when the twist angle is  $\pi/2$ , and instead of annihilation, they form

\*These authors contributed equally to this work.

†Contact author: q.wang@nju.edu.cn

‡Contact author: phmxiao@whu.edu.cn

§Contact author: liuhui@nju.edu.cn

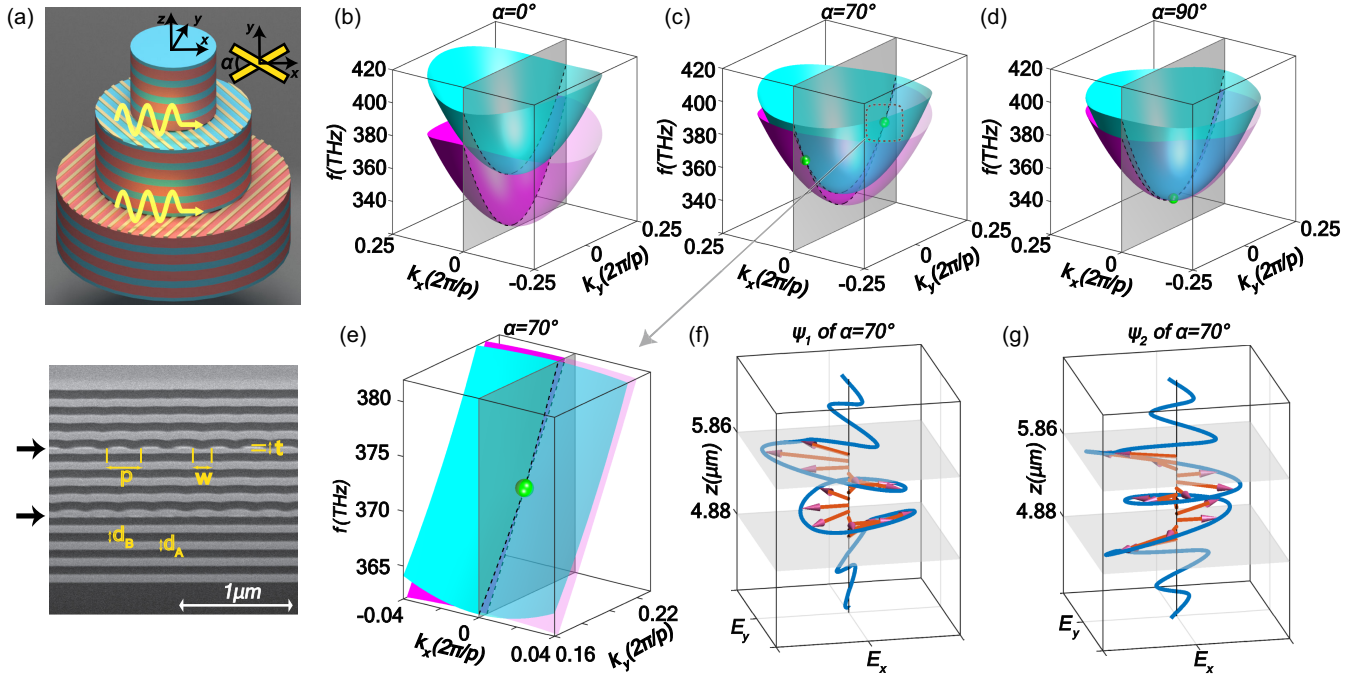


FIG. 1. (a) Schematic of twist bilayer metasurfaces embedded in 1D PCs (upper panel) and SEM image of the cross section of the structure (lower panel), the black arrows indicate the metasurfaces,  $p$ ,  $w$ , and  $t$  denote, respectively, the period, groove, and thickness of the nanostripes. (b)–(d) Dispersion of the TBAISs at different twist angles, the green dots stand for Dirac points. (e) Enlargement at the type-II Dirac point corresponding to the dashed region in (c). (f)–(g) Eigenfunctions of the TBAISs of  $\alpha = 70^\circ$  at Dirac points.

a charge-2 Dirac node at the crossing point [38]. We note that, the isofrequency contours at the type-II Dirac nodes are similar to the contours of the uniaxial medium, thus our system support 2D uniaxial interface waves that exhibit birefringence effects. The above results were experimentally verified in samples with different twist angles. The twist angle here can be considered as a new synthetic dimension. Over the past decade, constructing synthetic dimensions as new controllable degree of freedom has gained intense attention across various fields [40]. Our Letter provides a novel and flexible method to tune TDs through twisting, extending the use of synthetic dimensions as an effective knob for tuning topological semimetal phases. Furthermore, the uniaxial interface waves are applicable in phase matching, mode division, and photonic integration.

*Theory of topological degeneracy induced by symmetry breaking*—As depicted in Fig. 1(a), the TBAIS is constructed from two anisotropic metasurfaces (parallel golden bars), which are sandwiched by three 1D PCs. Each metasurface supports one AIS, and two AISs couple with each other through the central PC. The metasurfaces are made of gold nanostripes, whose period (200 nm) is much smaller than the working wavelength ( $> 800$  nm), and it can be modeled as a homogenous hyperbolic medium [41,42]. The two metasurfaces can twist relative to each other with an angle  $\alpha$ , and the coordinate axis are defined as the two diagonal directions [inset in Fig. 1(a)]. The 1D PCs are made of Ta2O5 and SiO2 with thickness  $d_A$  and  $d_B$ ,

respectively [lower panel of Fig. 1(a)]. The unit cell of the PC in between the metasurfaces is chosen as the  $A/2 - B - A/2$  configuration and the number of unit cells is 4, while the two outer PCs are in the  $B - A$  configuration. The above design ensures that the AISs only exist between the metasurfaces and the middle PC [43]. The two AISs interact with each other via evanescent waves and form TBAISs. These TBAISs possess mirror symmetry with respect to the central plane only at  $\alpha = 0^\circ$  and no mirror symmetry otherwise.

The dispersion of TBAISs is obtained by the transfer matrix method [44]. For AIS at a single metasurface, the dispersion is written as  $E = E_0 + ak_x^2 + bk_y^2$ , with  $a \neq b$  indicating the anisotropy of AISs,  $E_0$  being the frequency at  $k = 0$ . We assume that the eigenfield of the AISs are approximated by that at the  $\Gamma$  point (which is a reasonably good approximation around the  $\Gamma$  point, as shown in Figs. S4 and S5 [44]). From this, the angular-dependent coupling between the two AISs is derived by calculating the eigenfields overlap between them, and accordingly, the effective Hamiltonian is [44]:

$$\begin{aligned}
 H = & \frac{1}{2} [E_0 + (a+b)(k_x^2 + k_y^2) + (a-b)(k_x^2 - k_y^2) \cos \alpha] \cdot \sigma_0 \\
 & + (a-b)k_x k_y \sin \alpha \cdot \sigma_3 \\
 & + q \left[ \cos \alpha + \frac{1}{2} [(k_x^2 + k_y^2) \cos \alpha + k_x^2 - k_y^2] \right] \cdot \sigma_1, \quad (1)
 \end{aligned}$$

where  $\sigma_i (i = 0, 1, 2, 3)$  stands for the identity matrix and Pauli matrices. Note here the second term ( $\sigma_3$ ) describes the frequency detuning induced by twist between two uncoupled AISs, while the last term ( $\sigma_1$ ) stands the coupling strength between the two AISs, and  $q$  is regarded approximately as a constant. Considering the condition of  $0^\circ \leq \alpha \leq 90^\circ$ , for  $k_x = 0$ , the second term vanishes and the coefficient before the last term in Eq. (1) is  $q[\cos \alpha + \frac{1}{2}k_y^2(\cos \alpha - 1)]$ . There are three cases: (i) The system is up-down mirror-symmetric, i.e.,  $\alpha = 0^\circ$ , and the term  $(\cos \alpha - 1)$  equals to zero. Then the coupling strength remains positive regardless of  $k_y$ . Consequently, no TD can be found in this case. (ii) The mirror symmetry is broken by a twist ( $0^\circ < \alpha < 90^\circ$ ), then  $\cos \alpha$  is positive and  $(\cos \alpha - 1)$  is negative. At  $k_y = \pm\sqrt{2\cos \alpha/(1 - \cos \alpha)}$ , the third term in Eq. (1) equals zero. Therefore, there are two TDs formed at these two points. For  $90^\circ < \alpha < 180^\circ$ , another two TDs at  $(\pm\sqrt{2\cos \alpha/(1 - \cos \alpha)}, 0)$  are also found following a similar derivation. (iii) At  $\alpha = 90^\circ$ , two TDs merge. In conclusion, the TDs only emerge when the twist breaks the mirror symmetry in TBAISs.

Figure 1(b) plots the dispersion of the TBAISs with  $\alpha = 0^\circ$ , these two bands are gapped with NO TDs. When the mirror symmetry is broken by a twist (e.g.,  $\alpha = 70^\circ$ ), these two bands intersect with each other at  $(k_x, k_y) = (0, k_y^{TD})$ , as shown in Fig. 1(c). An enlarged view of one degenerate point is shown in Fig. 1(e). It is clear that the TD tilts in momentum space forming a type-II Dirac

point since the tilting parameter is larger than unity [44,47]. Figures 1(f) and 1(g) show the typical horizontal electric field  $(E_x, E_y)$  of the two states forming the Dirac point at  $\alpha = 70^\circ$ .

When further increasing the twist angle, the two type-II Dirac points move towards to the center of the momentum space, i.e.,  $\Gamma$  point. At  $\alpha = 90^\circ$  (where the two metasurfaces are perpendicular), these two type-II Dirac points merge into one TD with quadratic dispersions at the  $\Gamma$  point. This TD is classified as a charge-2 Dirac point, which characterized by a  $2\pi$  Berry phase when enclosing the DP [44]. Notably, the electric fields are parallel to the nanostripes in a single AIS, therefore these two AISs decouple at the charge-2 Dirac point when  $\alpha = 90^\circ$ .

*Observation of topological degeneracies with tuned twist angles*—To experimentally demonstrate the above symmetry-breaking induced TDs, a series of samples with different twist angles is fabricated [44]. It is known that multilayer structure suffers from the inevitable loss, however, the loss term here is approximated as an identity matrix and the DPs remain intact [44]. An SEM image of the cross section for one sample is shown in the lower panel of Fig. 1(a). In experiments, we measured the reflection spectrum along different directions across the  $\Gamma$  point, thus mapping the dispersion in the 2D momentum space [48].

Figure 2(a) shows the sketch of measuring dispersion of the TBAISs at  $\alpha = 70^\circ$ , where a type-II Dirac point is expected. Four measured reflection spectra at different azimuthal angles  $\theta$  for this sample are plotted in Fig. 2(b).

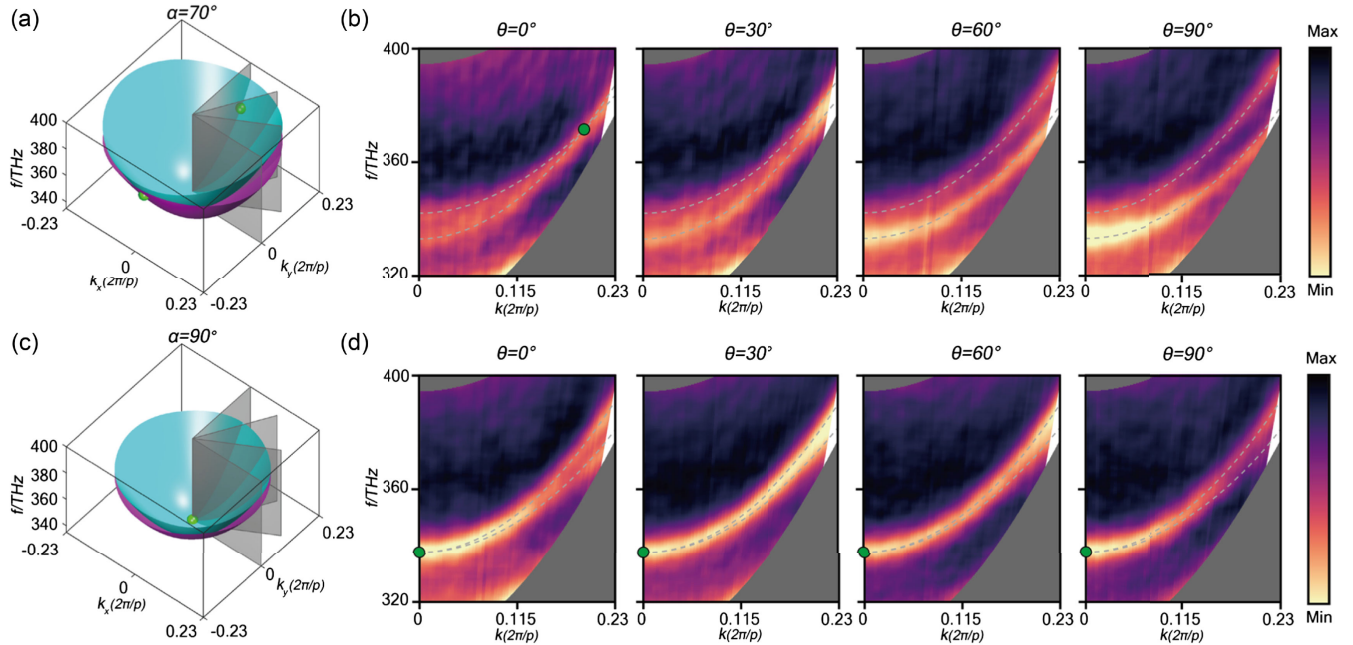


FIG. 2. (a) and (c) The schematics of dispersion at  $\alpha = 70^\circ$  and  $90^\circ$ , respectively. The degeneracies are denoted by the green dots, and the vertical gray planes indicate the azimuthal angles measured in experiment. (b) and (d) The reflection spectra at azimuthal angles  $\theta = 0^\circ, 30^\circ, 60^\circ, 90^\circ$ , respectively, where the dashed lines correspond to the dispersion obtained theoretically, and the gray shaded areas correspond to projected passband of the 1D PCs.

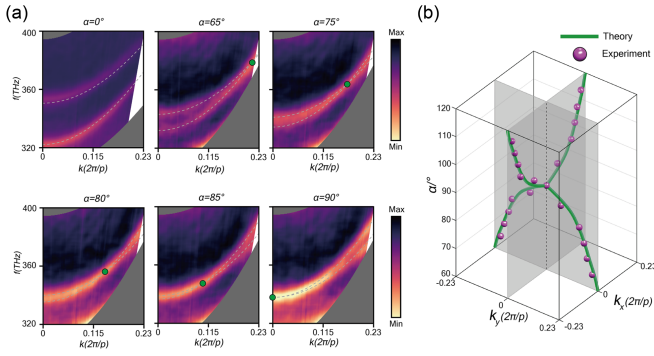


FIG. 3. (a) Reflection spectra along the  $k_y$  axis at different twist angles  $\alpha = 0^\circ, 65^\circ, 75^\circ, 80^\circ, 85^\circ,$  and  $90^\circ$ , where the dashed lines correspond to the theoretical dispersion, and the gray shaded areas corresponds to the projected passband of the 1D PCs. (b) Theoretical nodal chain (green solid line) and corresponding experimental results (magenta solid dots).

The TBAIS is manifested as reflection dips in our measurement. It is clear that two reflection dip lines intersect with each other at  $\theta = 0^\circ$  (i.e., along the  $k_y$  axis); while for the other three directions, these two dip lines are always separated, i.e., gapped. Figure 2(c) shows the corresponding dispersion with  $\alpha = 90^\circ$ , where a charge-2 Dirac point presents at the  $\Gamma$  point, the dispersions are quadratic, consistent with the effective Hamiltonian. For comparison, theoretical dispersions are shown in Figs. 2(b) and 2(d) with gray dashed lines, and the Dirac points are denoted by green dots, which match well with the measured results. The above results confirm the observation of the type-II Dirac point and the charge-2 Dirac point on the TBAISs.

According to the above discussion, these TDs are located on the  $k_y$  axis for  $0^\circ \leq \alpha \leq 90^\circ$ , and on the  $k_x$  axis otherwise. Subsequently, the measured reflection spectra along  $k_y$  axis at different twist angles  $\alpha$  are given in Fig. 3(a). We note that the theoretical TDs marked as the green dots move towards to the  $\Gamma$  point as twist angle  $\alpha$  increases; and they eventually merge into a charge-2 Dirac point at  $\alpha = 90^\circ$ . Meanwhile, there is no TD at  $\alpha = 0^\circ$  as the two reflection dip lines are separated. Taking the twist angle as a synthetic dimension, these TDs form a nodal chain in the 3D space consisting of  $k_x, k_y,$  and  $\alpha$ , with a chain point at  $(k_x, k_y, \alpha) = (0, 0, \pi/2)$ . For  $0 \leq \alpha \leq \pi/2$ , with expanded Hamiltonian around the chain point, these TDs are located at

$$k_y = \pm \sqrt{2(\pi/2 - \alpha)}, \quad k_x = 0. \quad (2)$$

We collect all the band crossing point in Fig. 3(a) and replot them in the  $(k_x, k_y, \alpha)$  space in Fig. 3(b). TDs that found in the experiment are marked as solid magenta dots, which agree well with the theoretically predicted nodal chain (green solid line). Thus, we have experimentally confirmed a chained nodal line in the synthetic space.

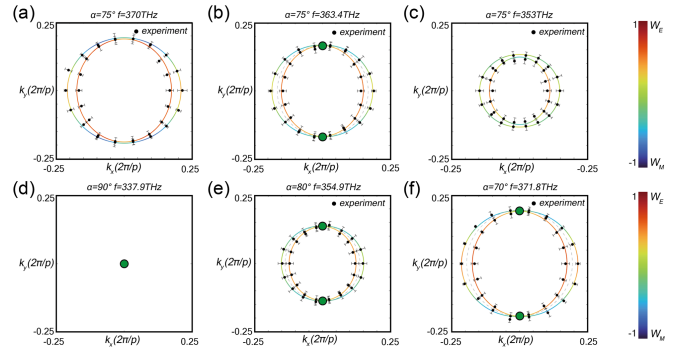


FIG. 4. (a)–(c) are the isofrequency contours above, at, and below the Dirac point of twist angle  $\alpha = 75^\circ$ , where the black dots represent the experimental measured dips. The color bar is given by  $(W_{E_z}^2 - W_{M_z}^2)/(W_{E_z}^2 + W_{M_z}^2)$ , where  $W_{E_z} = \int D_z E_z / 2 \cdot dz$  and  $W_{H_z} = \int B_z H_z / 2 dz$  stand for the electric and magnetic energies along the  $z$  axis. (d)–(f) are the isofrequency contours at the Dirac points of different twist angles.

*Uniaxial isofrequency contours at topological degeneracies*—In optics, the isofrequency contours plays a decisive role in various effects, including birefringence and negative refraction. In Figs. 4(a)–4(c), we show the isofrequency contours above, at, and below the TDs of the TBAISs at  $\alpha = 75^\circ$ . For clarity, the analytical isofrequency contours are plotted with colored lines, where the color denotes the polarization ratio of the corresponding eigenmode. It is observed that the inner (outer) contours are mainly dominated by  $E_z(H_z)$  near TDs, leading to a polarization difference between these two contours. We note that the isofrequency contour at the TD [Fig. 4(b)] is quite similar to those in a uniaxial crystal. Unlike conventional uniaxial medium where the isofrequency contours are intersected by a circle (ordinary waves) and an ellipse (extraordinary waves), here the contours of TBAISs are composed of two elliptical-like contours, indicating that both modes are extraordinary. Such a unique feature implies that the TBAISs can host the intriguing birefringent effect when the wave is incident from a structure with isotropic isofrequency contour. To be specific, when light is injected along the optical axis, i.e., TD, the two excited states propagate with the same direction; once deviating from the optical axis, the light beam splits into two with different directions [44]. Furthermore, the uniaxial interface waves of TBAIS can also be tuned by the twist angle, as depicted in Figs. 4(d)–4(f). To the best of our knowledge, this is the first time that the tunable birefringent effect has been demonstrated within localized interface waves, which favors applications in integrated mode division, phase matching for interface waves and more.

*Summary and outlook*—The properties of TBAISs were investigated both theoretically and experimentally. Twist between two metasurfaces breaks the up-down mirror symmetry of the system and leads to TDs. Specifically,

type-II and charge-2 Dirac points are observed experimentally. Subsequently, a nodal chain is formed in the  $k_x - k_y - \alpha$  synthetic space as confirmed by experiment. Our findings enrich the field of twist photonics [9] and may offer a potential route to demonstrating non-Abelian braiding by introducing more layers and twist angles [49–51]. Our Letter not only demonstrates the new possibility of creating TDs by breaking certain symmetries, but also presents a rather simple and flexible platform for manipulating the polarization and propagation of interface waves.

*Acknowledgments*—This work was financially supported by the National Natural Science Foundation of China Grants No. 12334015, No. 92163216, No. 92150302, No. 62288101, No. 12321161645, and No. 12274332, the Fundamental Research Funds for the Central Universities (No. 2024300369), the Natural Science Foundation of Jiangsu Province (No. BK20233001) and National Natural Science Fund for Excellent Young Scientists Fund Program (Overseas).

H. L. and M. X. proposed and designed the system. H. P. ran the numerical simulations. H. P. and X. W. carried out the experiment. M. X., Q. W., S. N. Z., and H. L. supervised the project. H. P., M. X., Q. W., and H. L. co-wrote the manuscript. All the authors contributed to the analysis and discussion of the results. H. P. and Q. W. contributed equally to this work.

- 
- [1] S. Shabani, D. Halbertal, W. J. Wu, M. X. Chen, S. Liu, J. Hone *et al.*, Deep moire potentials in twisted transition metal dichalcogenide bilayers, *Nat. Phys.* **17**, 720 (2021).
- [2] C. H. Jin, E. C. Regan, A. M. Yan, M. I. B. Utama, D. Q. Wang, S. H. Zhao *et al.*, Observation of moiré excitons in WSe<sub>2</sub>/WS<sub>2</sub> heterostructure superlattices, *Nature (London)* **567**, 76 (2019).
- [3] Y. Cao, V. Fatemi, S. Fang, K. Watanabe, T. Taniguchi, E. Kaxiras, and P. Jarillo-Herrero, Unconventional superconductivity in magic-angle graphene superlattices, *Nature (London)* **556**, 43 (2018).
- [4] R. Bistritzer and A. H. MacDonald, Moire bands in twisted double-layer graphene, *Proc. Natl. Acad. Sci. U.S.A.* **108**, 12233 (2011).
- [5] Z. Song, Z. Wang, W. Shi, G. Li, C. Fang, and B. A. Bernevig, All magic angles in twisted bilayer graphene are topological, *Phys. Rev. Lett.* **123**, 036401 (2019).
- [6] G. Tarnopolsky, A. J. Kruchkov, and A. Vishwanath, Origin of magic angles in twisted bilayer graphene, *Phys. Rev. Lett.* **122**, 106405 (2019).
- [7] S. Wu, Z. Y. Zhang, K. Watanabe, T. Taniguchi, and E. Y. Andrei, Chern insulators, van Hove singularities and topological flat bands in magic-angle twisted bilayer graphene. *Nat. Mater.* **20**, 488 (2021).
- [8] S. Yves, E. Galiffi, X. Ni, E. M. Renzi, and A. Alù, Twist-induced hyperbolic shear metasurfaces, *Phys. Rev. X* **14**, 021031 (2024).
- [9] J. L. Chen, X. Lin, M. Y. Chen, T. Low, H. S. Chen, and S. Y. Dai, A perspective of twisted photonic structures, *Appl. Phys. Lett.* **119**, 240501 (2021).
- [10] L. J. Du, M. R. Molas, Z. H. Huang, G. Y. Zhang, F. Wang, and Z. P. Sun, Moire photonics and optoelectronics, *Science* **379**, eadg0014 (2023).
- [11] S. A. Dyakov, N. S. Salakhova, A. V. Ignatov, I. M. Fradkin, V. P. Panov, J. K. Song, and N. A. Gippius, Chiral light in twisted Fabry-Pérot cavities, *Adv. Opt. Mater.* **12**, 2302502 (2024).
- [12] H. Hong, C. Huang, C. Ma, J. Qi, X. Shi, C. Liu, S. Wu, Z. Sun, E. Wang, and K. Liu, Twist phase matching in two-dimensional materials, *Phys. Rev. Lett.* **131**, 233801 (2023).
- [13] J. Guan, J. T. Hu, Y. Wang, M. J. H. Tan, G. C. Schatz, and T. W. Odom, Far-field coupling between moire photonic lattices, *Nat. Nanotechnol.* **18**, 514 (2023).
- [14] H. Y. Wang, W. Xu, Z. Y. Wei, Y. Y. Wang, Z. S. Wang, X. B. Cheng *et al.*, Twisted photonic Weyl meta-crystals and aperiodic Fermi arc scattering, *Nat. Commun.* **15**, 2440 (2024).
- [15] K. Dong, T. Zhang, J. Li, Q. Wang, F. Yang, Y. Rho, D. Wang, C. P. Grigoropoulos, J. Wu, and J. Yao, Flat bands in magic-angle bilayer photonic crystals at small twists, *Phys. Rev. Lett.* **126**, 223601 (2021).
- [16] B. Lou, N. Zhao, M. Minkov, C. Guo, M. Orenstein, and S. Fan, Theory for twisted bilayer photonic crystal slabs, *Phys. Rev. Lett.* **126**, 136101 (2021).
- [17] P. Wang, Y. L. Zheng, X. F. Chen, C. M. Huang, Y. V. Kartashov, L. Torner, V. V. Konotop, and F. W. Ye, Localization and delocalization of light in photonic moire lattices, *Nature (London)* **577**, 42 (2020).
- [18] H. N. Tang, F. Du, S. Carr, C. Devault, O. Mello, and E. Mazur, Modeling the optical properties of twisted bilayer photonic crystals, *Light Sci. Appl.* **10**, 157 (2021).
- [19] L. Huang, W. Zhang, and X. Zhang, Moire quasibound states in the continuum, *Phys. Rev. Lett.* **128**, 253901 (2022).
- [20] H.-Y. Luan, Y.-H. Ouyang, Z.-W. Zhao, W.-Z. Mao, and R.-M. Ma, Reconfigurable moire nanolaser arrays with phase synchronization, *Nature (London)* **624**, 282 (2023).
- [21] S. Liu, S. J. Ma, R. W. Shao, L. Zhang, T. Yan, Q. Ma, S. Zhang, and T. J. Cui, Moire metasurfaces for dynamic beamforming, *Sci. Adv.* **8**, eabo1511 (2022).
- [22] H. N. Tang, B. C. Lou, F. Du, M. J. Zhang, X. Q. Ni, W. J. Xu, R. Jin, S. H. Fan, and E. Mazur, Experimental probe of twist angle-dependent band structure of on-chip optical bilayer photonic crystal, *Sci. Adv.* **9**, eadh8498 (2023).
- [23] X. Zhang, C. Bian, Z. Gong, R. Chen, T. Low, H. Chen, and X. Lin, Hybrid surface waves in twisted anisotropic hetero-metasurfaces, *Phys. Rev. Appl.* **21**, 064034 (2024).
- [24] G. W. Hu, Q. D. Ou, G. Y. Si, Y. J. Wu, J. Wu, Z. G. Dai *et al.*, Topological polaritons and photonic magic angles in twisted  $\alpha$ -MoO<sub>3</sub> bilayers, *Nature (London)* **582**, 209 (2020).
- [25] M. Z. Hasan and C. L. Kane, Colloquium: Topological insulators, *Rev. Mod. Phys.* **82**, 3045 (2010).
- [26] Y. Ando and L. Fu, Topological crystalline insulators and topological superconductors: From concepts to materials, *Annu. Rev. Condens. Matter Phys.* **6**, 361 (2015).

- [27] N. P. Armitage, E. J. Mele, and A. Vishwanath, Weyl and Dirac semimetals in three-dimensional solids, *Rev. Mod. Phys.* **90**, 015001 (2018).
- [28] B. H. Yan and C. Felser, Topological materials: Weyl semimetals, *Annu. Rev. Condens. Matter Phys.* **8**, 337 (2017).
- [29] L. Lu, Z. Y. Wang, D. X. Ye, L. X. Ran, L. Fu, J. D. Joannopoulos, and M. Soljacic, Experimental observation of Weyl points, *Science* **349**, 622 (2015).
- [30] L. Lu, L. Fu, J. D. Joannopoulos, and M. Soljacic, Weyl points and line nodes in gyroid photonic crystals, *Nat. Photonics* **7**, 294 (2013).
- [31] M. Kim, Z. Jacob, and J. Rho, Recent advances in 2D, 3D and higher-order topological photonics, *Light Sci. Appl.* **9**, 130 (2020).
- [32] A. B. Khanikaev and G. Shvets, Two-dimensional topological photonics, *Nat. Photonics* **11**, 763 (2017).
- [33] C. K. Chiu, J. C. Y. Teo, A. P. Schnyder, and S. Ryu, Classification of topological quantum matter with symmetries, *Rev. Mod. Phys.* **88**, 035005 (2016).
- [34] C. K. Chiu and A. P. Schnyder, Classification of reflection-symmetry-protected topological semimetals and nodal superconductors, *Phys. Rev. B* **90**, 205136 (2014).
- [35] S. A. Yang, H. Pan, and F. Zhang, Dirac and Weyl superconductors in three dimensions, *Phys. Rev. Lett.* **113**, 046401 (2014).
- [36] A. Bansil, H. Lin, and T. Das, Colloquium: Topological band theory, *Rev. Mod. Phys.* **88**, 021004 (2016).
- [37] T. Ozawa, H. M. Price, A. Amo, N. Goldman, M. Hafezi, L. Lu *et al.*, Topological photonics, *Rev. Mod. Phys.* **91**, 015006 (2019).
- [38] S. Vaidya, J. Noh, A. Cerjan, C. Jörg, G. von Freymann, and M. C. Rechtsman, Observation of a charge-2 photonic Weyl point in the infrared, *Phys. Rev. Lett.* **125**, 253902 (2020).
- [39] H. Z. Wu, Z. Z. Liu, and J. J. Xiao, Synthetic Weyl points in plasmonic chain with simultaneous inversion and reflection symmetry breaking, *Phys. Rev. B* **110**, 075420 (2024).
- [40] L. Q. Yuan, Q. Lin, M. Xiao, and S. H. Fan, Synthetic dimension in photonics, *Optica* **5**, 1396 (2018).
- [41] P. Cheben, R. Halir, J. H. Schmid, H. A. Atwater, and D. R. Smith, Subwavelength integrated photonics, *Nature (London)* **560**, 565 (2018).
- [42] A. Poddubny, I. Iorsh, P. Belov, and Y. Kivshar, Hyperbolic metamaterials, *Nat. Photonics* **7**, 948 (2013).
- [43] M. Kaliteevski, I. Iorsh, S. Brand, R. A. Abram, J. M. Chamberlain, A. V. Kavokin, and I. A. Shelykh, Tamm plasmon-polaritons: Possible electromagnetic states at the interface of a metal and a dielectric Bragg mirror, *Phys. Rev. B* **76**, 165415 (2007).
- [44] See Supplemental Material at <http://link.aps.org/supplemental/10.1103/PhysRevLett.134.106601>, which includes Refs. [45,46], for detailed derivation and simulation.
- [45] A. Yariv, *Photonics: Optical Electronics in Modern Communications* (Oxford University Press, Oxford, 2007).
- [46] Q. Wang, M. Xiao, H. Liu, S. Zhu, and C. T. Chan, Measurement of the Zak phase of photonic bands through the interface states of a metasurface/photonic crystal, *Phys. Rev. B* **93**, 041415(R)(2016).
- [47] C. Hu, Z. Li, R. Tong, X. Wu, Z. Xia, L. Wang, S. Li, Y. Huang, S. Wang, B. Hou, C. T. Chan, and W. Wen, Type-II Dirac photons at metasurfaces, *Phys. Rev. Lett.* **121**, 024301 (2018).
- [48] C. Jörg, S. Vaidya, J. Noh, A. Cerjan, S. Augustine, G. Von Freymann, and M. C. Rechtsman, Observation of quadratic (charge-2) Weyl point splitting in near-infrared photonic crystals, *Laser Photonics Rev.* **16**, 2100452 (2022).
- [49] Q. S. Wu, A. A. Soluyanov, and T. Bzdusek, Non-Abelian band topology in noninteracting metals, *Science* **365**, 1273 (2019).
- [50] Y. Yang, B. Yang, G. C. Ma, J. S. Li, S. Zhang, and C. T. Chan, Non-Abelian physics in light and sound, *Science* **383**, eadf9621 (2024).
- [51] E. Yang, B. Yang, O. B. You, H. C. Chan, P. Mao, Q. H. Guo, S. Ma, L. Xia, D. Fan, Y. Xiang, and S. Zhang, Observation of non-Abelian nodal links in photonics, *Phys. Rev. Lett.* **125**, 033901 (2020).